Reaction and Quenching of $Cl(^2P_j)$ Atoms in Collisions with Methane and Deuterated Methanes

Yutaka Matsumi, Keisuke Izumi, Vladimir Skorokhodov,† Masahiro Kawasaki,* and Noriyuki Tanaka‡

Institute for Electronic Science and Graduate School of Environmental Science, Hokkaido University, Sapporo 060, Japan

Received: July 11, 1996; In Final Form: November 11, 1996⊗

Bimolecular rate constants for the reaction of ground-state $Cl(^2P_{3/2})$ atoms and for quenching of excited spin−orbit state $Cl^*(^2P_{1/2})$ atoms in collisions with CH_4, CD_4, and CH_2D_2 have been measured at room temperature. Chlorine atoms were produced by the photolysis of CCl_2F_2 and HCl at 193 nm and monitored by the technique of laser-induced fluorescence at the vacuum ultraviolet region. The rate constants for the reaction of Cl atoms were found to be as follows: CH_4, $(10.0 \pm 1.0) \times 10^{-14}$; CH_2D_2, $(7.0 \pm 0.8) \times 10^{-14}$; and CD_4, $(8.2 \pm 1.0) \times 10^{-15}$ cm^3 molecule^{-1} s^{-1}. The absolute second-order rate constants for the removal of Cl* atoms were as follows: CH_4, $(3.0 \pm 0.3) \times 10^{-11}$; CH_2D_2, $(1.1 \pm 0.1) \times 10^{-10}$; and CO_2, $(1.2 \pm 0.1) \times 10^{-11}$ cm^3 molecule^{-1} s^{-1}. The removal of Cl* atoms was shown to proceed mainly by collisional quenching.

Introduction

The reaction of atomic chlorine with methane

$$Cl(^2P) + CH_4 \rightarrow HCl + CH_3 \qquad (1)$$

is important in atmospheric chemistry since both species play discernible roles in stratospheric processes. This reaction is considered to be the principal pathway in which chlorine atoms are removed from the ozone-destroying ClO_x cycle.[1] Methane, the most abundant organic species in both the troposphere and the stratosphere, is one of the major greenhouse gases in the atmosphere, and its concentration has steadily increased by about 1% per year for the past 150 years,[2] although this rate has been significantly reduced in the last 5 years.[3] To establish a global methane budget and strengths of various natural and anthropogenic sources of methane is clearly important in order to understand future climate changes.

The various CH_4 sources demonstrate characteristic carbon and hydrogen isotopic compositions due to different CH_4 formation processes.[2,4] The relative contribution of the sources to the global methane isotopic budget can be found by comparing these characteristic isotopic fingerprints with the mean isotopic composition. To calculate the isotopic budget by this approach, the isotopic fractionation of methane removal through its major sinks, including reaction 1, must be known. Reaction 1 possesses a carbon kinetic isotope effect[5,6] that results in an influence on the $^{13}CH_4/^{12}CH_4$ isotopic composition. Meanwhile, the influence of reaction 1 on deuterium enrichment for methane isotopic composition cannot be accurately evaluated since the absolute rate constants of the reaction of $Cl(^2P)$ with deuteriomethanes have remained poorly evaluated.

Reaction 1 is also a representative of hydrogen-atom-abstraction reactions, and its kinetics have been studied extensively.[7−13] Nevertheless, a direct measurement of the individual rate constant k_1 for deuteriomethane isotopomers other than CH_4 has never been reported in the literature. The only indirect method[7] used to determine a rate constant ratio for CH_4 and CD_4 was to irradiate a mixture of Cl_2 and this pair of methane isotopomers with UV light in a static cell over a temperature range of 300−475 K. Mass-spectrometrical analysis of the isotopic composition of the products permitted a determination of the ratio of the rate constants.[7] More recently, it was found that in collisions with CH_4 and various other partners, the rate constants for the removal of the ground $Cl(^2P_{3/2})$ and excited $Cl^*(^2P_{1/2})$ spin−orbit states differ significantly.[14,15] The reactivities of the Cl* and Cl states, which demonstrate a spin−orbit splitting of 881 cm^{-1}, are suspected to be considerably different.[16] There has been considerable study of spin−orbit effects in reactions of halogen atoms, and in most reactions studied, the ground spin−orbit state $^2P_{3/2}$ is more reactive than the $^2P_{1/2}$ state due to the adiabatic nature of the corresponding potential surfaces.[17] It is now recognized that the large body of rate data for $Cl(^2P)$ obtained in earlier studies did not correctly differentiate between the Cl and Cl* states.[10,13,18] Hence, the different reactivities of the Cl and Cl* states in reaction 1 could account for the nonlinear Arrhenius behavior experimentally observed in a number of studies.[10,13] From a more fundamental standpoint, reaction 1 is important in chemical reaction dynamics studies. Recent experimental[12,19−21] and theoretical[22−25] studies have focused on deriving the product internal-state and angular-scattering distributions in the $Cl(^2P_{3/2}) + CH_4$ reaction.

The present study has been undertaken in order to obtain the absolute rate constants for the reaction of Cl and Cl* atoms with deuterated methanes at room temperature. Using the technique of vacuum UV laser-induced fluorescence (LIF), we were able to monitor both Cl and Cl* spin−orbit states and derive separately the rate coefficients for their removal in collisions with reactant partners. This approach allows us to elucidate the different reactivities of the Cl and Cl* states in collisions with the deuterated methane isotopomers.

Experimental Section

The present investigations were carried out using an experimental apparatus that has been described in detail previously.[26] A brief description of the setup is provided here, with emphasis on the facets most important to this study. All experiments were carried out under slow-flow conditions. A gas mixture consisting of a Cl, Cl* atom precursor, reactant, and buffer gases

† Present address: Institute of Physics, St. Petersburg State University, Petrodvorets, St. Petersburg 198904, Russia.

‡ Graduate School of Environmental Science.

⊗ Abstract published in *Advance ACS Abstracts,* January 15, 1997.

S1089-5639(96)02064-6 CCC: $14.00

flowed through a reaction cell. The precursor component was dissociated at 193 nm by pulsed laser light. After a delay between the dissociation and probe laser pulses, the Cl or Cl* atoms were probed by vacuum UV LIF.

The dissociation laser used in the experiments was an ArF excimer laser with typical output of 20 mJ/pulse at 10-Hz repetition rate. Chlorine atoms were generated by the photolysis of HCl and CCl_2F_2 precursors. Photodissociation of HCl at 193 nm produces Cl and Cl* states with the branching ratio Cl*/Cl = 0.50.[14,26,27] Thus, photolysis of HCl allowed us to investigate the kinetics of the reactions for atoms in both the ground Cl and excited Cl* states. CCl_2F_2 photolysis was not exploited in our study of the reactions of excited Cl* atoms since only a minor amount of chlorine atoms are formed in this state.[28]

In the present study, two allowed transitions of the Cl and Cl* states were used for the vacuum UV LIF monitoring, namely, 4s $^2P_{3/2} \leftarrow$ 3p $^2P_{3/2}$ and 4s $^2P_{1/2} \leftarrow$ 3p $^2P_{1/2}$ at λ = 134.724 and 135.166 nm,[26] respectively. The tunable probe vacuum UV light was generated by four-wave mixing ($2\omega_1 - \omega_2$) in Kr gas using two dye lasers pumped by a single XeCl excimer laser (λ = 308 nm).[29] The wavelength of ω_1 was 212.56 nm, which corresponded to a two-photon resonance to the Kr 5p[1/2]$_0$ state, and the wavelength of ω_2 was tuned near 500 nm. Typical laser energies were 0.5 and 5 mJ/pulse for ω_1 and ω_2, respectively. The ω_1 and ω_2 light beams were focused with a lens (f = 200 mm) into a cell containing Kr gas at 15−20 Torr. The generated vacuum UV light beam passed through a LiF window, propagated through a reaction cell, and then a part of the beam was reflected by a LiF beam splitter into a vacuum UV monochromator equipped with a solar blind photomultiplier tube in order to monitor the vacuum UV light intensity.

The vacuum UV LIF signal of the Cl or Cl* states was detected by a second solar blind photomultiplier mounted at right angles to the propagation direction of the probing light and the λ = 193-nm dissociating laser beam. The time delay between the dissociation and probe laser pulses was controlled by a pulse generator (SRS DG535), and the jitter of the delay time was less than 10 ns. In typical experiments, the delay time was scanned to cover the whole time domain of the fluorescence signal decay, usually t = 0−3 ms (with step Δt = 15 μs) for the Cl and t = 0−30 μs (Δt = 0.15 μs) for the Cl*. At each step, the signal was averaged for 10 laser shots, and the total time of the decay profile measurements was 200 s.

The sample gas mixtures were prepared directly in storage bulbs by premixing the precursor (HCl or CCl_2F_2), a reactant gas, and Ar as a buffer gas. The gases used in the experiments had the following stated purities and were obtained from HCl, 99.9%, CCl_2F_2, 99.9%, CH_4, 99.99%, and Ar, 99.999%. The deuterated methanes CH_2D_2 and CD_4 were from Matheson Co. with the stated isotopic contents of 98 and 99.2 atom % D, respectively. All gases were used without further purification.

Results

A. Rate Constants for the Reaction of Cl($^2P_{3/2}$) with CH_4, CH_2D_2, and CD_4. In these experiments, photolysis of both HCl and CCl_2F_2 precursors was used as a source of ground-state Cl atoms. All experiments were carried out under pseudo-first-order conditions with an excess of reactant partner diluted with Ar as a buffer gas. A typical ratio of partial pressures in the sample gas mixture was P(precursor):P(reactant):P(Ar) = 2:18:720 with a total pressure of 740 Torr. In the present experiments, the total pressure of the gas mixture in the reaction cell was varied in the 8−80 Torr range so that the partial pressure of the reactant gas was varied over the range 0.2−2 Torr and the range of partial pressures of the Cl precursor was 0.02−0.2 Torr. An excess of the buffer gas in the sample mixture provided a fast thermalization of the translationally hot nascent Cl, Cl* atoms generated by the precursor photolysis.

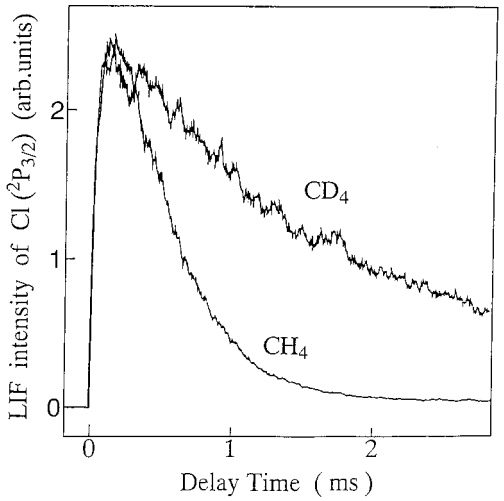

Figure 1. Typical temporal profiles of ground-state Cl atoms in the presence of methane isotopomers. Data obtained with the CCl_2F_2 precursor at a methane pressure of 0.5 Torr; total pressure of the sample gas mixture was 20 Torr.

Figure 1 shows typical temporal profiles for the decay of the Cl state. The time-resolved vacuum UV LIF signal of the Cl atoms produced by the photolysis of HCl exhibits a fast rise (t < 10−20 μs) followed by a slow decay. This rapid rise represents the contribution of collisional quenching of the excited Cl* atoms generated by photolysis to the ground Cl state. At the reagent gas pressure used, the collisional quenching of Cl* atoms was entirely completed on a time scale much shorter than that for the reaction of the Cl. This means that in the longer time domain with t > 0.05−0.1 ms, essentially single-exponential decay was observed.

The temporal behavior of Cl atoms in the long time domain was governed by the following processes:

$$\mathrm{Cl}(^2\mathrm{P}_{3/2}) + \mathrm{CH}_{4-n}\mathrm{D}_n \rightarrow \mathrm{HCl(DCl)} + \mathrm{CH}_{3-n'}\mathrm{D}_{n'} \quad (2)$$

$$\mathrm{Cl}(^2\mathrm{P}_{3/2}) \xrightarrow{k_d} \text{loss (by diffusion and gas mixture flow)} \quad (3)$$

The second reactant on the left side of reaction 2 represents one of the deuteriomethane isotopomers. To experimentally verify the insignificance of other secondary chemical processes that might affect the Cl atom decay, we varied both the photolyzing laser energies by a factor of 4 and the sample gas mixture ratios by a factor of 2. The measured rate constants were independent of these two experimental parameters.

Since our experiments were carried out under conditions where only processes 2, and 3 could contribute to the Cl time profile, the data were fitted using the following equation:

$$[\mathrm{Cl}] = A \exp(-k_2[\mathrm{CH}_{4-n}\mathrm{D}_n] - k_d)t = A \exp(-k_2' t) \quad (4)$$

and the pseudo-first-order rate constant k_2' for a particular reactant pressure was derived by a nonlinear least-squares fit. The resulting dependence of k_2' on the pressure of the reactant species is shown in Figure 2. The nonzero intercepts corresponding to zero reactant pressure result from Cl atoms escaping from the probing region because of diffusion and gas mixture flow. The experimental dependence in Figure 2 was fitted with a linear function, and the k_2 bimolecular rate constants were derived from the slope of the best-fit straight lines. The rate

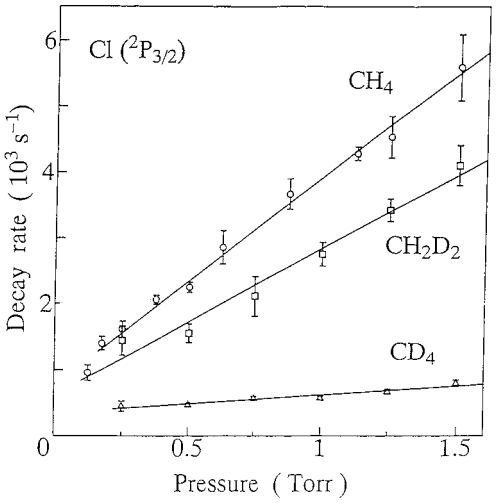

Figure 2. Second-order plot for the removal of ground-state Cl atoms in the reaction with methane isotopomers. The total pressure of the sample gas mixture was varied in order to change the methane isotopomer pressure; CCl_2F_2 precursor was used.

TABLE 1: Reaction Rate Constants for Cl + Methanes at 298 K

	$10^{14}k_2$, cm^3 molecule^{-1} s^{-1}	
methane	this work	refs
CH_4	10.0 ± 1.0	10.0[a]
CH_2D_2	7.0 ± 0.8	
CD_4	0.82 ± 0.10	0.92[b]

[a] Reference 13. [b] For CH_4-CD_4 isotopomers, $k_H/k_D = 10.9$ at 304.4 K, ref 7.

constants obtained are presented in Table 1. The uncertainties of the rate constants in the present study for Cl and Cl* states include both the statistical imprecision (1 standard deviation) originating from a random scattering of experimental points and the systematic errors in measurements of partial and total pressures.

B. Rate Constants for the Removal of Cl*($^2P_{1/2}$) in Collisions with CH_4, CH_2D_2, and CO_2. In the present experiments, the excited Cl* atoms were generated by the photolysis of HCl at $\lambda = 193$ nm. The typical sample gas mixture was the same as described in subsection A. An excess of the buffer Ar gas had a negligible influence on the Cl* decay profiles due to the very low quenching efficiency of Ar: $(3.0 \pm 1.0) \times 10^{-16}$ cm^3 molecule^{-1} s^{-1}.[30]

A typical time profile presenting the decay of the Cl* state is shown in Figure 3. The observed vacuum UV LIF time profile of Cl* after a photolyzing pulse displays a LIF detector limited rapid rise within 0.6 μs that is followed by a relatively slower decay in the 20-μs short time domain. This decay entirely matches the fast rise in the vacuum UV LIF signal of the Cl state as shown in Figure 3. In the short time domain, the temporal behavior of Cl* should be expressed by the following processes:

$$Cl^*(^2P_{1/2}) + CH_{4-n}D_n \rightarrow Cl(^2P_{3/2}) + CH_{4-n}D_n \quad (4a)$$

$$Cl^*(^2P_{1/2}) + CH_{4-n}D_n \rightarrow HCl\ (DCl) + CH_{3-n'}D_{n'} \quad (4b)$$

Accordingly, the Cl* decay profiles were fitted with a single-exponential function to obtain the pseudo-first-order rate constant $k'_4 = (k_{4a} + k_{4b})[CH_{4-n}D_n] + k_d$. The resulting k'_4 values are plotted in Figure 4 along with a linear fit to the data. The removal rate constants $k_4 = k_{4a} + k_{4b}$ derived from the slopes of these fits are given in Table 2.

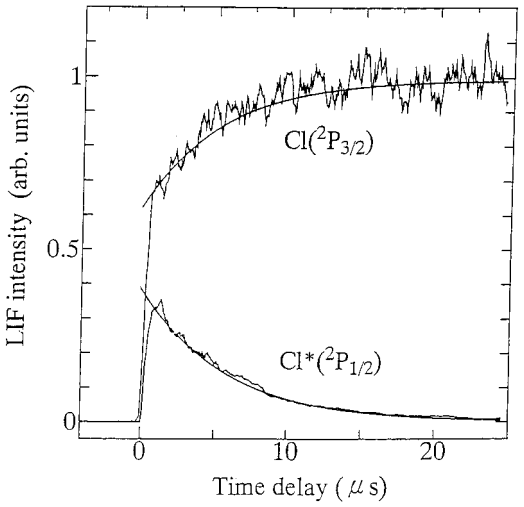

Figure 3. Temporal profiles of excited Cl* and ground Cl states in the presence of 0.27 Torr of CH_4 with fitted exponential functions. The decay of Cl* matches the rise of Cl (see text).

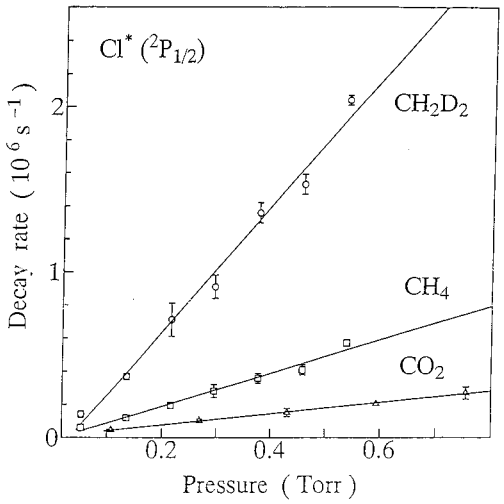

Figure 4. Second-order plot for the removal of excited-state Cl* atoms in collisions with methane isotopomers and CO_2. The total pressure of the sample gas mixture was varied in order to change the reactant gas pressure.

TABLE 2: Collisional Relaxation Rate Constants for the Spin−Orbit State Cl*($^2P_{1/2}$): Cl*($^2P_{1/2}$) + M → Cl($^2P_{3/2}$) + M[a]

	$10^{11}k_4$, cm^3 molecule^{-1} s^{-1}			
M	this work	refs	ν, cm^{-1}	ΔE, cm^{-1}
CH_4	3.0 ± 0.3	2.2 ± 0.3[b]	$\nu_4 = 1306$	425
CH_2D_2	11 ± 1		$\nu_4 = 1033$	152
			$\nu_7 = 1090$	209
CF_4		2.3 ± 0.3[b]	$\nu_1 = 909$	28
		2.7 ± 0.8[c]		
CCl_2F_2		$(3.3 \pm 0.5) \times 10$[b]	$\nu = 915$	34
		$(1.8 \pm 0.4) \times 10$[c]		
CO_2	1.2 ± 0.1	1.5 ± 0.4[d]	$\nu_2 = 667$	−214
Ar		$(3.0 \pm 1.0) \times 10^{-5}$ [b]		

[a] Energy defects ΔE were obtained as following: $\Delta E = \nu_i - E_{SO}(Cl)$, where ν_i is the fundamental frequency of the quencher and $E_{SO}(Cl)$ is the spin−orbit splitting Cl*($^2P_{1/2}$) − Cl($^2P_{3/2}$) = 881 cm^{-1}. [b] Reference 30. [c] Reference 15. [d] Reference 34.

From the experimental decay profiles, only the overall removal rate constant $k_4 = k_{4a} + k_{4b}$ can be derived, since both channels, i.e., quenching (4a) and reaction (4b), contribute to the removal of Cl* atoms. One can see in Figure 3 that the temporal profile of the Cl ground state measured under the same experimental conditions is fit well with an exponential function

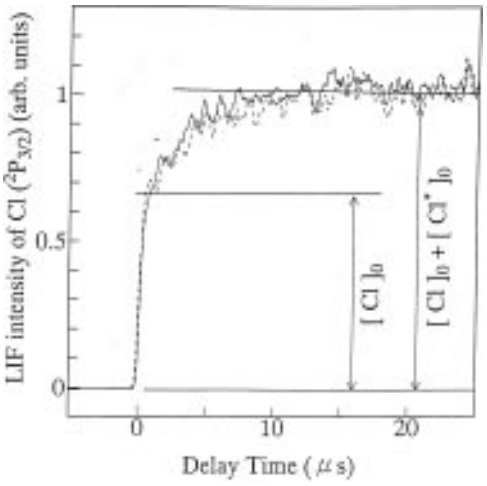

Figure 5. Temporal profiles of the ground Cl state in the presence of 0.27 Torr of CH_4 (solid line) or 0.54 Torr of CO_2 (broken line). Horizontal lines correspond to the initial concentration of ground-state Cl atoms and to the sum of the initial concentrations of both Cl and excited-state Cl* atoms. Data were obtained for the sample gas mixtures (see text) at a total pressure of 10 Torr.

$(1 - \exp(-k_4't))$. Comparing the Cl and Cl* profiles in Figure 3, it appears that the quenching channel (4a) provides a major contribution to the Cl* removal, while the reaction channel (4b) is a minor one.

In a special set of experiments, we made an attempt to evaluate the loss of Cl* atoms due to reaction (4b). In these experiments, we analyzed the behavior of the Cl temporal profiles in the presence of CH_4 or CO_2 in the short time domain. The pressures of the CH_4 or CO_2 species were chosen so that the removal rates of Cl* were comparable. Figure 5 illustrates this approach. Analyzing the temporal profile observed in the photolysis of the $HCl/CH_4/Ar$ mixture, we first found the initial value of the Cl ground-state signal (corresponding to the $[Cl]_0$ initial concentration) by fitting this profile as mentioned above. Then, using the well-known branching ratio $Cl^*/Cl = 0.50$[14,26,27] for HCl photolysis at 193 nm, we could estimate the expected signal corresponding to the total $[Cl]_0 + [Cl^*]_0$ initial amount of chlorine atoms. This value is presented by a horizontal line plotted in Figure 5. Since there is no appreciable deviation in Figure 5, we can conclude that the Cl, Cl* atom loss is smaller than the experimental error in the time profile measurements. Similar results were obtained for the $HCl/CO_2/Ar$ mixture photolysis. Observing the Cl decay profiles in the long time domain in these experiments, we found a very low efficiency of the $Cl + CO_2$ reaction. Thus, the Cl temporal profile in the short time domain should reflect only spin−orbit relaxation of Cl* due to quenching by CO_2 without any loss of Cl, Cl* atoms. Close overlapping of the time profiles measured for the mixtures with CH_4 and CO_2 means that the overall Cl + Cl* loss is less than our experimental accuracy estimated as ±10−12%. On the other hand, in the HCl photolysis, we produced an appreciable amount of Cl* atoms (33% of the total Cl + Cl* amount), yet we see no observable Cl + Cl* loss. This allows us to conclude that in collisions of Cl* with CH_4, the reaction channel (4b) is of minor importance in comparison with quenching (4a). Unfortunately, the present approach does not allow an evaluation of the k_{4b} constant with reasonable uncertainty in order to compare the reactivities of Cl and Cl* with CH_4 because of the limited experimental accuracy and fast quenching of Cl* via the dominant (4a) channel. From our data, we can only provide an upper limit of the rate constant for reaction (4b). Since the ratio of Cl* loss in (4b) to the initial amount of Cl* is equal to the $k_{4b}/(k_{4a} + k_{4b})$ ratio and taking the upper limit of the Cl* loss as 10%, we can derive $k_{4b} < k_4(10\%/33\%) = 10^{-11}$ cm^3 molecule^{-1} s^{-1}. Further experimental studies with monitoring of the HCl product in reaction (4b) are needed to perform comparisons of the reactivities of the Cl and Cl* states in the reaction with CH_4.

Discussion

The rate constant of the Cl reaction with CH_4 has been the subject of a number of studies using different experimental techniques. As a result, this rate constant can be considered to be well evaluated[13] with a recommended value of 1.0×10^{-13} cm^3 molecule^{-1} s^{-1} obtained by taking a mean value from the most reliable rate coefficient studies. Our k_2 rate constant for CH_4 is in agreement with the recommended value. For reaction 1 with CD_4, the ratio k_H/k_D of the rate constants for the CH_4 and CD_4 reactants has only been indirectly measured previously.[7] The ratios k_H/k_D at temperatures ranging from 300 to 475 K were obtained mass-spectrometrically by analyzing the isotopic composition of the stable products CH_3Cl and CD_3Cl formed in secondary radical reactions with Cl_2 molecules. Although this indirect experimental technique could not distinguish between the reactions of ground Cl and Cl* state atoms, the reported rate constant ratio $k_H/k_D = 10.9(\pm 0.8)$ at 304.4 K is in good agreement with the present value of $k_2(CH_4)/k_2(CD_4) = 12.2 \pm 0.9$ at room temperature. Since the reaction is dominated by tunneling,[23−25] the kinetic isotope effect is large even at room temperature. Recently, Espinosa-Garcia and Corchado[31] reported the results of their theoretical calculation, $k_2(CH_4)/k_2(CD_4) = 41.79$ at 300 K.

As for the variation of k_2 with partial or total deuterium substitution of hydrogen atoms, the rate constants decrease monotonically with the number of D atoms in the reactant. It is well-known that the mechanism giving rise to changes in k_2 on deuterium substitution includes differences in the zero-point energies (ZPEs) of the isotopomers and greater quantum mechanical tunneling for hydrogen. Differences in the ZPEs make activation energies higher for reactants containing D atoms rather than H atoms and reduce the reaction rate constants. Together with the experimental results in this study, we present our computational results for the kinetic isotope effect in reaction 2 obtained using the empirical bond-energy−bond-order (BEBO) method.[32] A simplified linear three-atom model for the activated complex was used in these calculations, and the reactants and products were considered to be an atom + diatomic molecule. The calculated $k_2(CH_{4-n}D_n)/k_2(CH_4)$ ratios and the experimental points are given in Figure 6. The calculated points lie very close to the linear dependence on deuterium substitution. In contrast to this, the experimental points show discernible declining from this dependence with deviations considerably exceeding our experimental errors. The experimental points cannot be extrapolated with an ordinary linear dependence that usually fits the kinetic data quite well in similar systems. This nonlinearity indicates that deuterium substitution in reaction 2 cannot be described as a simple additive, so-called primary isotope effect. Further theoretical studies of the present reaction system are needed to evaluate all the factors mentioned above and gain some insight into the nature of the observed isotope effect.

Nevertheless, since more than 99% of the partially deuterated methane in the atmosphere is CH_3D, the reaction rate constant of CH_3D should virtually control the D content in atmospheric methane in terms of methane destruction with Cl. Assuming that the reaction rate constants of CH_4 and CD_4 obtained in this study are representative of H-abstraction (k_H) and D-abstraction (k_D) rate constants, respectively, one can evaluate

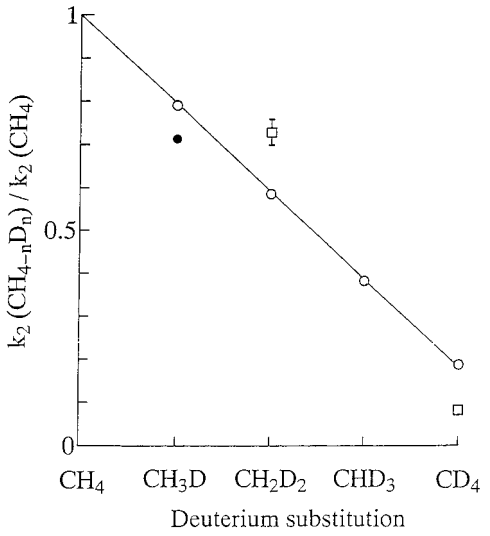

Figure 6. Dependence of the rate constant ratio $k_2(CH_{4-n}D_n)/k_2(CH_4)$ in the reaction of methane isotopomers with $Cl(^2P_{3/2})$ on the extent of deuterium substitution. Open circles with extrapolated line present results of BEBO calculations; solid circle presents *ab initio* calculations (ref 32). Experimental results of the present study are given by squares with error bars.

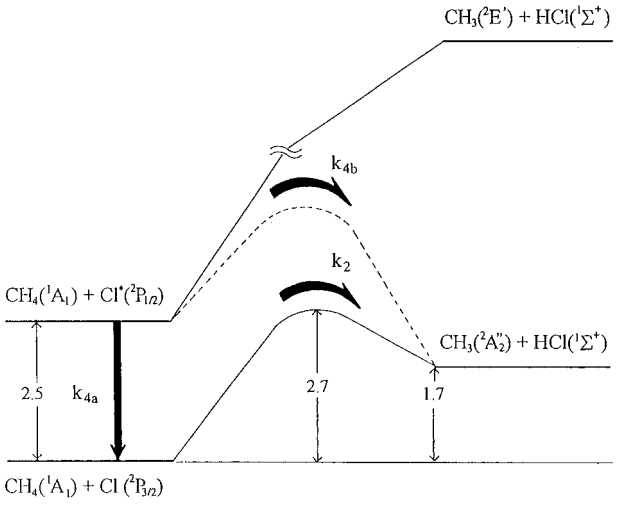

Figure 7. Energy diagram for the reaction $Cl(^2P_j) + CH_4 \rightarrow HCl + CH_3$. Numbers in the figure are activation energies and heats of reaction (in kcal/mol) taken from ref 38 at room temperature. Solid lines indicate adiabatic correlations between electronic states of reactants and products.

the reaction rate constant for CH_3D as $0.25k_D + 0.75k_H = 0.77 \times 10^{-13}$ cm^3 molecule^{-1} s^{-1}, with the resulting kinetic fractionation effect of hydrogen isotope in the atmospheric methane destruction reaction with Cl being $k_2(CH_4)/k_2(CH_3D) = 10^{-13}/0.77 \times 10^{-13} = 1.3$. This value is very close to our computational result of $[k_2(CH_3D)/k_2(CH_4)]^{-1} = 1.25$ obtained with the BEBO method. On the other hand, *ab initio* molecular orbital calculations for the ratio are reported to be 1.47.[33]

The Cl* removal rate constants k_4 are given in Table 2 along with published values. The obtained rate constant $(3.0 \pm 0.3) \times 10^{-11}$ cm^3 molecule^{-1} s^{-1} for the Cl* state removal by CH_4 is in good agreement with the recently reported value of $(2.2 \pm 0.3) \times 10^{-11}$ cm^3 molecule^{-1} s^{-1} [30] and in evident disagreement with the value $(3.9 \pm 0.8) \times 10^{-12}$ cm^3 molecule^{-1} s^{-1} measured by Clark and Husain.[16] For removal by CO_2, our rate constant along with the confidence interval $(1.2 \pm 0.1) \times 10^{-11}$ cm^3 molecule^{-1} s^{-1} lies within the stated interval of experimental errors for the $(1.5 \pm 0.4) \times 10^{-11}$ cm^3 molecule^{-1} s^{-1} value published previously[34] but far away from the $<5 \times 10^{-13}$ cm^3 molecule^{-1} s^{-1} estimate of Clark and Husain.[16] The causes which could affect the values measured in ref 16 have been discussed earlier, that is, the possibility of nonequilibration of the hyperfine levels, etc.[30,35]

Table 2 shows the electronic quenching rate constants of $Cl^*(^2P_{1/2})$ to $Cl(^2P_{3/2})$ with various collision partners M, some selected vibrational modes of M, and energy gaps ΔE that are the minimum energies possible for excitation of a fundamental vibration in the collision partner M. The listed fundamental vibrations within 300 cm^{-1} of the excitation energy of the Cl* spin−orbit state can be considered to be active modes for the quasi-resonant electronic-to-vibrational E → V energy transfer processes. However, a simple view of this table does not suggest the straightforward relaxation process through E → V energy-transfer. For example, CF_4 and CCl_2F_2 species demonstrate similar ΔE values, but corresponding k_4 rate constants differ by more than an order of magnitude. The k_4 constants for the CH_4, CF_4, and CO_2 molecules are very close to each other, but their ΔE values vary significantly. The CH_2D_2 and CCl_2F_2 species also demonstrate comparable k_4 constants close to the gas kinetic value and essentially different energy defects ΔE. A more correct interpretation of these k_4 and ΔE variations, however, can be based on the Fermi golden rule. It dictates that the transition probability is a function of both an interaction matrix element and a density of states. Since the interaction matrix element depends strongly on the shape of the potential energy surfaces for the $Cl(^2P_j)$ + M collision partners,[36] the simple energy gap law proposed previously[15,30,34] does not work for the Cl* quenching process.

Comparison of the data for the CH_4 and CH_2D_2 isotopomers demonstrates a considerable increase of the k_4 rate constant for the CH_2D_2 species. This high rate constant indicates a high efficiency of the nonreactive spin−orbit quenching of the Cl* state by CH_2D_2. In comparison to the $Cl(^2P_j) + CH_4$ system, CH_2D_2 has a vibrational mode closer to the Cl* electronic excitation energy and also a higher rotational level density than CH_4; accordingly, the quenching rate constant k_4 of CH_2D_2 is larger than that of CH_4.

Both reactive and nonreactive collisions of $Cl(^2P_j)$ atoms with CH_4 can be considered in terms of the energy diagram proposed in Figure 7. Symmetry considerations indicate that for the $Cl(^2P_j) + CH_4$ system, only one doublet potential energy surface, correlating with the ground Cl state, adiabatically leads to the $HCl(X^1\Sigma^+) + CH_3(^2A_2'')$ products in their ground electronic states. The other surface also originating from the Cl + CH_4 reactants (absent in Figure 7) and the surface corresponding to the Cl* + CH_4 reactants correlate adiabatically with the products in the excited electronic states,[10] which are inaccessible for thermal energies at room temperature. Although the reaction channel for Cl* + CH_4 is exothermic, this reaction may only occur by nonadiabatic crossing in the manifold of appropriate potential energy surfaces correlating with the reactants or the products. The experimentally observed low efficiency of the Cl* + CH_4 reaction channel can mean that the nonadiabatic pathway to the product valley remains inefficient. In this connection, it is interesting to mention the effect of the spin−orbit fine structure on the cumulative reaction probability of Cl with HCl reported by Schatz.[37] With his realistic quantum reactive scattering calculations for an open-shell atom + diatom system, he found that Cl + HCl is very much in the adiabatic limit with respect to the correlation between asymptotic and saddle-point electronic states. The effect of spin−orbit splitting is to shift the reaction threshold up in energy for the excited $Cl(^2P_{1/2})$ spin−orbit state, and as a consequence, in this limit,

the thermal rate constants is completely dominated by the $Cl(^2P_{3/2})$ reaction channel.

References and Notes

(1) *Scientific Assessment of Stratospheric ozone*; WMO: Geneva, 1990. *Atmospheric Ozone 1985*; WMO: Geneva, 1986.

(2) Wahlen, M. *Annu. Rev. Earth Planet. Sci.* **1993**, *21*, 407. Mroz, E. J. *Chemosphere* **1993**, *26*, 45.

(3) Matsueda, H.; Inoue, H. Y.; Ishii, M.; Nogi, Y. *Geochem. J.* **1996**, *30*, 1.

(4) Bergamaschi, P.; Schupp, M.; Harris, G. W. *Appl. Opt.* **1994**, *33*, 7704.

(5) Tanaka, N.; Xiao, Y.; Lasaga, A. C. *J. Atm. Chem.*, in press.

(6) Saueressig, G.; Bergamaschi, P.; Growley, J. N.; Fischer, H. *Geophys. Res. Lett.* **1995**, *22*, 1225.

(7) Chiltz, G.; Eckling, R.; Goldfinger, P.; Huybrechts, G.; Johnston, H. S.; Meyers, L.; Verbeke, G. *J. Chem. Phys.* **1963**, *38*, 1053.

(8) Lin, C. L.; Leu, M. T.; DeMore, W. B. *J. Phys. Chem.* **1978**, *82*, 1772.

(9) Zahniser, M. S.; Berquist, B. M.; Kaufman, F. *Int. J. Chem. Kinet.* **1978**, *10*, 15.

(10) Ravishankara, A. R.; Wine, P. H. *J. Chem. Phys.* **1980**, *72*, 25.

(11) Dobis, O.; Benson, S. W. *Int. J. Chem. Kinet.* **1987**, *19*, 691.

(12) Simpson, W. R.; Orr-Ewing, A. J.; Zare, R. N. *Chem. Phys. Lett.* **1993**, *212*, 163.

(13) DeMore, W. B.; Sander, S. P.; Golden, D. M.; Hampson, R. F.; Kurylo, M. J.; Howard, C. J.; Ravishankara, A. R.; Kolb, C. E.; Molina, M. J. In *JPL Publication* 94−26; Jet Propulsion Laboratory: Pasadena, CA, 1994.

(14) Park, J.; Lee, Y.; Flynn, G. W. *Chem. Phys. Lett.* **1991**, *186*, 441; **1992**, *192*, 138.

(15) Chichinin, A. I.; Krasnoperov, L. N. *Chem. Phys. Lett.* **1989**, *160*, 448.

(16) Clark, R. H.; Husain, D. *J. Chem. Soc., Faraday Trans. 2* **1984**, *80*, 97.

(17) Dagdigian, P. J. *J. Chem. Rev.* **1987**, *87*, 1.

(18) Watson, R. T. *J. Phys. Chem. Ref. Data* **1977**, *7*, 621.

(19) Simpson, W. R.; Rakitzis, T. P.; Kandel, S. A.; Orr-Ewing, A. J.; Zare, R. N. *J. Chem. Phys.* **1995**, *103*, 7313.

(20) Simpson, W. R.; Rakitzis, T. P.; Kandel, S. A.; Lev-On, T.; Zare, R. N. *J. Phys. Chem.* **1996**, *100*, 7938.

(21) Valey, D. F.; Dagdigian, P. J. *J. Phys. Chem.* **1995**, *99*, 9843.

(22) Wang, X.; Ben-Nun, M.; Levine, R. D. *Chem. Phys.* **1995**, *197*, 1.

(23) Duncan, W. T.; Truong, T. N. *J. Chem. Phys.* **1995**, *103*, 9642.

(24) Gonzalez-Lafont, A.; Truong, T. N.; Truhlar, D. G. *J. Chem. Phys.* **1991**, *95*, 8873.

(25) Dobbs, K. D.; Dixon, D. A. *J. Phys. Chem.* **1994**, *98*, 12584.

(26) Tonokura, K.; Matsumi, Y.; Kawasaki, M.; Tasaki, S.; Bersohn, R. *J. Chem. Phys.* **1992**, *97*, 8210.

(27) Tiemann, E.; Kanamori, H.; Hirota, E. *J. Chem. Phys.* **1988**, *88*, 2457.

(28) Matsumi, Y.; Tonokura, K.; Kawasaki, M.; Inoue, G.; Satyapal, S.; Bersohn, R. *J. Chem. Phys.* **1991**, *94*, 2669; **1992**, *97*, 5261.

(29) Hilbig, R.; Wallenstein, R. *IEEE J. Quantum. Electron.* **1983**, *QE-19*, 1759.

(30) Tyndall, G. S.; Orlando, J. J.; Kegley-Owen, C. S. *J. Chem. Soc., Faraday Trans.* **1995**, *91*, 3055.

(31) Espinosa-Garcia, J.; Corchado, J. C. *J. Chem. Phys.* **1996**, *105*, 3517.

(32) Johnston, H. S. *Gas Phase Reaction Rate Theory*; Ronald: New York, 1966.

(33) Xiao, Y.; Tanaka, N.; Lasaga, A. C. To be published. Calculation details were reported in ref 5.

(34) Sotnichenko, S. A.; Bokun, V. Ch.; Nadkhin, A. I. *Chem. Phys. Lett.* **1988**, *153*, 560.

(35) Krasnoperov, L. N.; Chichinin, A. I. *Chem. Phys. Lett.* **1986**, *124*, 8.

(36) Aquilanti, V.; Cappelletti, D.; Pirani, F. *J. Chem. Soc., Faraday Trans.* **1993**, *89*, 1467.

(37) Schatz, G. C. *J. Phys. Chem.* **1995**, *99*, 7522.

(38) Atkinson, R.; Baulch, D. L.; Cox, R. A.; Hampson, R. F., Jr.; Kerr, J. A.; Troe J. *J. Phys. Chem. Ref. Data* **1992**, *21*, 1125.